



# Understanding novel biocomposites comprising of short cellulose fibres in a hybrid cellulose/silk fibroin matrix

James A. King<sup>a</sup>, Peter J. Hine<sup>a</sup>, Daniel L. Baker<sup>a</sup>, Yu Shi<sup>b</sup>, Xiaoling Liu<sup>c</sup>, Jiawen Lu<sup>c</sup>, Saihua Li<sup>c</sup>, Xiaoye Cong<sup>c</sup>, Michael E. Ries<sup>a</sup>,\*

<sup>a</sup> School of Physics and Astronomy, The University of Leeds, Leeds, LS2 9JT, West Yorkshire, UK

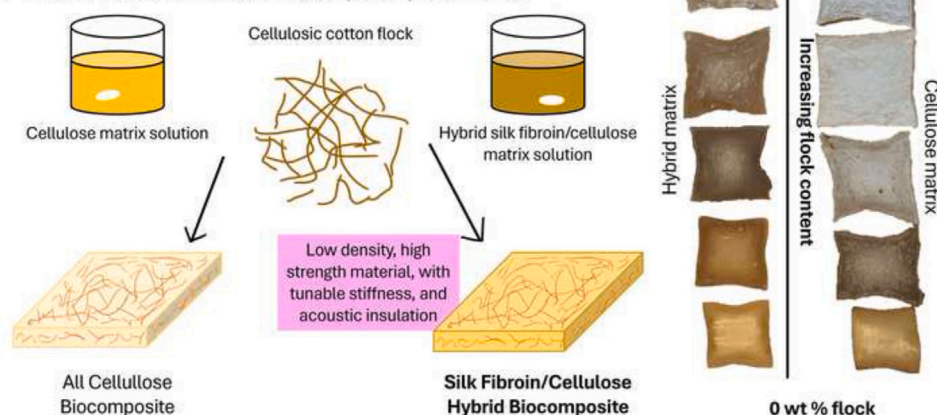
<sup>b</sup> Leeds Institute of Textiles and Colour, The University of Leeds, Leeds, LS2 9JT, West Yorkshire, UK

<sup>c</sup> Faculty of Science and Engineering, The University of Nottingham, Ningbo, 315100, Zhejiang, China

## GRAPHICAL ABSTRACT

### How can a hybrid blend matrix improve short-fibre reinforced biocomposites?

1. Hybrid matrix shows improved matrix-fibre adhesion and fibre loading.
2. Improved fibre loading increases maximum stress and strain at failure.
3. Short fibres used to produce low-density insulative composites.
4. Fibre content shown to dictate composite performance.



## ARTICLE INFO

Dataset link: <https://doi.org/10.5518/1751>

### Keywords:

Silk fibroin  
Cellulose  
Short fibre  
Composite  
Ionic liquid  
Biomaterial  
Biocomposite

## ABSTRACT

Biopolymer blends offer a promising route to tunable, high-performance biomaterials, yet their potential in reinforced composites remains underexplored. This study investigates biocomposites produced by reinforcing a hybrid biopolymer matrix (90:10 cellulose:silk fibroin) with randomly oriented short cotton fibres and varying the reinforcement weight percentage. A pure cellulose matrix was tested for comparison. The composites were characterised using X-ray diffraction (XRD), density analysis, tensile testing, optical microscopy, scanning electron microscopy (SEM), and acoustic insulation analysis. Optimal hybrid composites with 50 vol% reinforcement exhibited superior performance to pure cellulose, achieving a Young's modulus of  $3.3 \pm 0.3$  GPa, strain at failure of  $1.4 \pm 0.2\%$ , and maximum tensile strength of  $42 \pm 6$  MPa. These enhancements were attributed to the hybrid matrix's reduced viscosity and improved solvation capacity allowing higher fibre loading and stronger interfacial adhesion. In addition, the hybrid matrix's greater extensibility enabled more

\* Corresponding author.

E-mail addresses: [mmjki@leeds.ac.uk](mailto:mmjki@leeds.ac.uk) (J.A. King), [Xiaoling.Liu@nottingham.edu.cn](mailto:Xiaoling.Liu@nottingham.edu.cn) (X. Liu), [m.e.ries@leeds.ac.uk](mailto:m.e.ries@leeds.ac.uk) (M.E. Ries).

<https://doi.org/10.1016/j.compositesa.2025.109459>

Received 3 September 2025; Received in revised form 3 November 2025; Accepted 23 November 2025

Available online 25 November 2025

1359-835X/© 2025 The Authors. Published by Elsevier Ltd. This is an open access article under the CC BY license (<http://creativecommons.org/licenses/by/4.0/>).

efficient stress transfer to the fibres, maximising mechanical performance. Fibre content was identified as the primary driver of material modulus, underscoring the critical role of reinforcement. Flock content was then shown to correlate with improved acoustic insulation performance which led to a maximum average acoustic transmission loss of  $47 \pm 7$  dB in hybrid samples compared to  $29 \pm 4$  dB in cellulose samples. This work demonstrates the viability of hybrid biopolymer blends for creating low-density, high-performance materials from short-fibre textile waste with sustainable applications in insulative structural engineering.

## 1. Introduction

As concerns about environmental damage grow, the need for sustainable and effective replacements for traditional petroleum-based materials has become increasingly evident. Ideal solutions should be sustainably sourced, processable, biodegradable, and high-performance. Although synthetic polymers are widely used due to their low cost and uniformity, they are unsustainable, exhibit poor biocompatibility, and may produce toxic degradation products [1]. Biopolymers, such as cellulose and silk fibroin (SF), address these challenges and are thus of great interest.

Cellulose, the most abundant renewable resource on Earth, is a structural polysaccharide found in plants [1]. It consists of repeating anhydroglucose monomers (D-glucopyranose) in their lowest-energy ring conformation [2]. Extensive inter- and intramolecular hydrogen bonding, along with hydrophobic stacking, makes cellulose insoluble in water and capable of achieving extremely high strengths [3, 4]. SF is the structural protein which, alongside the glue-like silk sericin, forms silk fibres [5]. SF is composed primarily of glycine rich hexapeptide sequences. SF amino acid sequences vary, based on source and application, but always provides structural strength to silk materials [5].

Blending these two biopolymers has been shown to enhance material strength, stiffness, and biocompatibility [6–10]. Tian et al. showed with nuclear magnetic resonance studies that SF and cellulose were miscible due to hydrogen bonding encouraging molecular association [11]. This was supported by atomic force microscopy studies which indicated homogeneous blending [8,11,12]. In our previous work, we optimised hybrid films by composition to produce samples with improved modulus, strength, and flexibility due to increased molecular interactions and viscoelastic network relaxation facilitated by molecular slippage [13, 14].

Biopolymeric materials have also been optimised by inclusion of reinforcement in composites. These are materials formed of a dispersed phase of reinforcement and a continuous matrix phase which combine the properties of the two components [15]. All cellulose composites (ACCs) have chemically identical cellulose matrices and reinforcing fibres which differ only in their crystalline morphology and polymer alignment [7,15,16]. This design ensures superior matrix-reinforcement adhesion at interfaces and improved ease of recycling compared to traditional fibre reinforced polymer composites [15]. Fibre reinforced composites can be altered by changing the lengthscale and direction of reinforcement between: discontinuous, randomly oriented short fibres; linear aligned filaments; planar, two-dimensionally aligned, woven fabrics; and three dimensionally aligned, complex, woven, reinforcements [17]. Although higher level reinforcement offers improved strength, short fibre reinforcement reduces anisotropy, can have high mechanical performance, and allows for the use of waste textiles [15,17,18]. Hjelm et al. demonstrated effective use of post-consumer viscose textile waste with a thermoplastic binder matrix to create composites with a modulus of  $5 \pm 2$  MPa and scalable application in packaging [18].

Combining the concept of hybrid biopolymer blends with isotropic short fibre reinforcement offers a novel approach to repurposing waste materials into high-performance, circular materials. Natural fibre materials have good thermal insulation, acoustic insulation, and mechanical properties [19,20]. Victoria et al. demonstrated all-biopolymer composites of woven cotton can improve mechanical properties over the raw

material [15,21]. They achieved a Young's modulus of  $3.4 \pm 0.2$  GPa and an average tensile strength of  $72 \pm 2$  MPa: values comparable with some widely used stiff plastics [21]. Adapting these self-reinforcing composites (and optimising them with hybrid matrices) to utilise short-fibre reinforcement will allow for the direct use of post-consumer waste textiles. Energy use in building can be up to 40% of the total energy consumption in industrialised countries and improved insulative materials would reduce this environmental impact [22]. Use of natural textile waste avoids incineration of these materials while promoting carbon sequestering natural fibre industries, which have been adversely affected by synthetic fabric market growth [20,23,24].

In this study, we compare the performance of isotropically reinforced short fibre biocomposite sheets with cellulose and optimised hybrid matrices (90:10, cellulose:SF) to identify the value of hybrid biopolymers in reinforced biocomposites. We prepare composite samples by reinforcing biopolymer solutions with isotropically oriented cellulosic cotton flock and systematically vary the weight percentage of reinforcing cotton flock. We utilise ionic liquids as our solvent for biopolymer dissolution as a sustainable solvent with effective dissolution, recyclability, and minimal environmental impact [25–27]. We chose 1-ethyl-3-methylimidazolium acetate (EmimAc) and dimethyl sulfoxide (DMSO) as our solvent mixture based on the optimisation study previously performed for the dissolution of SF and cellulose [3].

X-ray diffraction (XRD) is used to establish the morphology and hence the fibre volume percentage of the composites. Gravimetric density analysis is then used to indicate the effect of increasing reinforcement content on processing conditions, resulting in decreasing density. The different matrices are compared to show the hybrid solutions give superior fibre interpenetration and adhesion. Tensile testing was then performed to show superior performance in samples with hybrid matrix due to improved extensibility, fibre loading, and fibre-matrix adhesion at interfaces. The experimental evidence is used to validate a model composite modulus prediction to allow future sample tunability. Characterisation with optical and scanning electron microscopy is used to confirm behaviours seen and discuss failure mechanisms. Lastly, the samples are characterised with acoustic insulation testing to indicate the applicability of these materials. The proposed composites are shown to produce valuable materials and indicate the importance of both biopolymer blends and short-fibre reinforcement for textile waste usage. This promising study provides motivation for future testing of these materials in structural applications with acoustic insulation needs, or in biomedical applications [1, 28–30].

## 2. Materials and methods

### 2.1. Materials

Avicel PH-101 microcrystalline cellulose was used as the cellulose source for dissolution to form the cellulose and hybrid matrices. Degummed *Bombyx mori* mulberry silk thread was purchased from Empress Mills (Colne, United Kingdom) for use as the SF source for dissolution to form the hybrid matrix. CD60 milled cotton flock was purchased from Goonvean (Devon, United Kingdom) for use as reinforcing short fibres in composite samples. The ionic liquid, 1-ethyl-3-methylimidazolium acetate (EmimAc), was purchased from Proionic (Raaba-Grumbach, Austria), with a purity of 97%. All EmimAc, cellulose, and silk was stored under dry conditions and dried overnight at

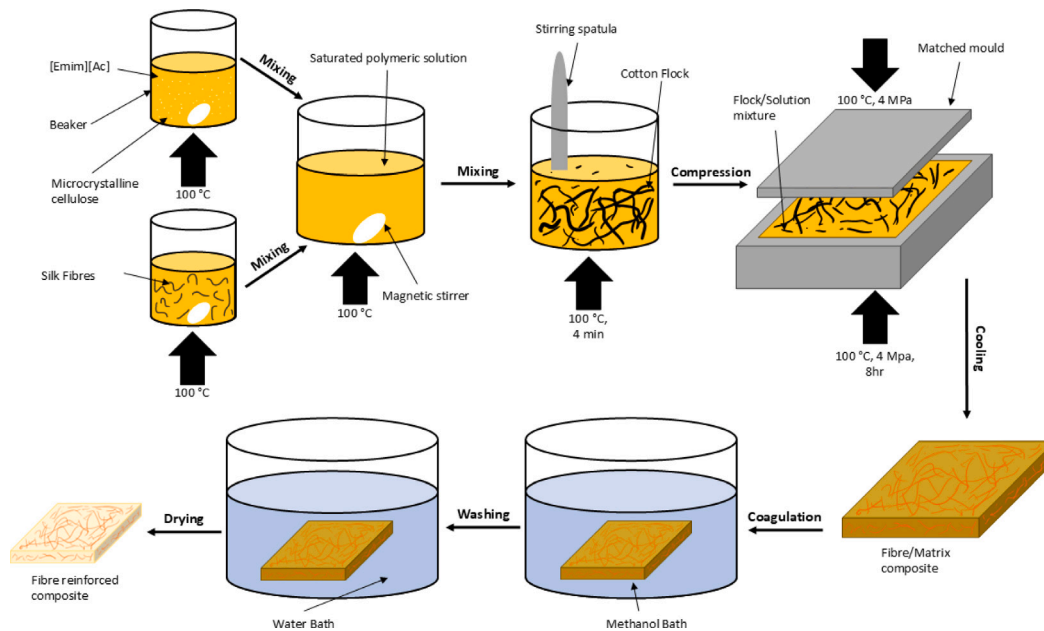


Fig. 1. Diagram indicating the production process for the composites with a hybrid matrix.

60 °C under vacuum before use. Dimethyl Sulfoxide (DMSO) was purchased from Sigma-Aldrich (Dorset, England) with a purity of 99.9%. Methanol was purchased from Fisher Scientific (Loughborough, United Kingdom), with purity of 98%, for coagulation of samples.

## 2.2. Composite fabrication

The hybrid solution of cellulose and silk fibroin was prepared with a 10% SF and 90% cellulose polymer composition, based on previous work indicating a peak in hybrid matrix performance between 5–15 wt% SF content [13]. The solvent ratio was selected based on previous studies on the effective dissolution of SF and cellulose with EmimAc and DMSO solvent mixtures [1,3,31]. A diagram of the production process can be seen in Fig. 1. Examples of samples at each processing stage can be seen in Figure S1.

Cellulose was dissolved at 10 wt% in a 20:80, EmimAc:DMSO mixture of solvents. Silk fibres were dissolved at 10 wt% in an 80:20, EmimAc:DMSO mixture of solvents. Polymeric solids were firstly dispersed in the relevant weight of DMSO, then stirred and preheated to 100 °C for 30 min. The relevant weight of EmimAc was preheated at 100 °C for 30 min then mixed with the dispersed solids in DMSO. Solutions were then stirred for 16 h, at 100 °C, at 200 rpm to produce pale yellow to dark amber transparent solutions. Hybrid solutions were prepared by mixing the SF and cellulose solutions at the required ratio for 30 min, at 100 °C and 200 rpm. All dissolution was performed in sealed vessels to reduce the effects of humidity on dissolution.

The polymer solution was then mixed with cotton flock for 5 min until the mixture was homogenous. Both flock and solution were preheated to 100 °C and stirred while heated at 100 °C. The mixture of undissolved flock and polymeric solution was then dispersed in matched moulds and compressed for 8 h at 4 MPa and 100 °C. This period and pressure was selected after a short optimisation study described in Figure S2 [15,21,32,33]. Samples were then removed from compression and allowed to cool to room temperature for 12 h. Samples were coagulated in a methanol bath for 24 h before washing in deionised water (5 l) for 48 h. The water was replaced twice in that period. Coagulated and washed samples were dried at room temperature and humidity for 6 hr. Samples were compressed between metal sheets ( $\approx 10$  KPa using bulldog clips), to alleviate deformation due to differential shrinkage during drying and cooling, then dried

for 24 h at 60 °C whilst still under compression. Sample thickness varied from 1.2–3.9 mm with increasing reinforcement correlating with reduced shrinkage as discussed in Section 3.2.

Before any characterisation, samples were equilibrated under ambient conditions for at least 24 h. The average room humidity was  $50 \pm 1\%$  and the average temperature was  $20.6 \pm 0.2$  °C. Analysis results were averaged over at least three measurements, unless otherwise mentioned, with errors calculated as the standard error. Examples of samples with cellulose and hybrid matrices can be seen in Fig. 2. Throughout this manuscript the reinforced samples with hybrid or cellulose matrices will be referred to as only hybrid or cellulose samples respectively.

## 2.3. Composite characterisation

### 2.3.1. Mechanical testing

Tensile tests of the films were carried out on an Instron 5564 universal test machine equipped with a 2 kN calibrated load cell at room temperature. Tests were performed on dumbbell shapes of type V according to ASTM D638. Dumbbell shapes were laser cut from the samples. The dumbbell shapes were approximately 60 mm in length and 3 mm in width at the thinnest point. The gauge length was 25–30 mm. Samples were gripped with sandpaper at clamping points to minimise slippage. The cross-head speed in the direction parallel to the sample was  $5 \text{ mm min}^{-1}$ . The tensile Young's modulus (in the initial linear strain range of 0.0–0.5%) was measured from the resulting stress strain curves. The strain at failure was taken as the strain at which the maximum stress was achieved and the gradient of the stress strain curve became negative.

The tensile stress was calculated by dividing the force by the average original cross-sectional area in the gauge length segment of the specimen [33]:

$$\sigma = \frac{F}{w \times d} \quad (1)$$

where  $\sigma$  is the stress in the sample  $F$  is the load (N),  $w$  is the width of the sample (mm), and  $d$  is the thickness of the sample (mm). The tensile strain was calculated using the equation [33]:

$$\epsilon = \frac{D}{L} \quad (2)$$



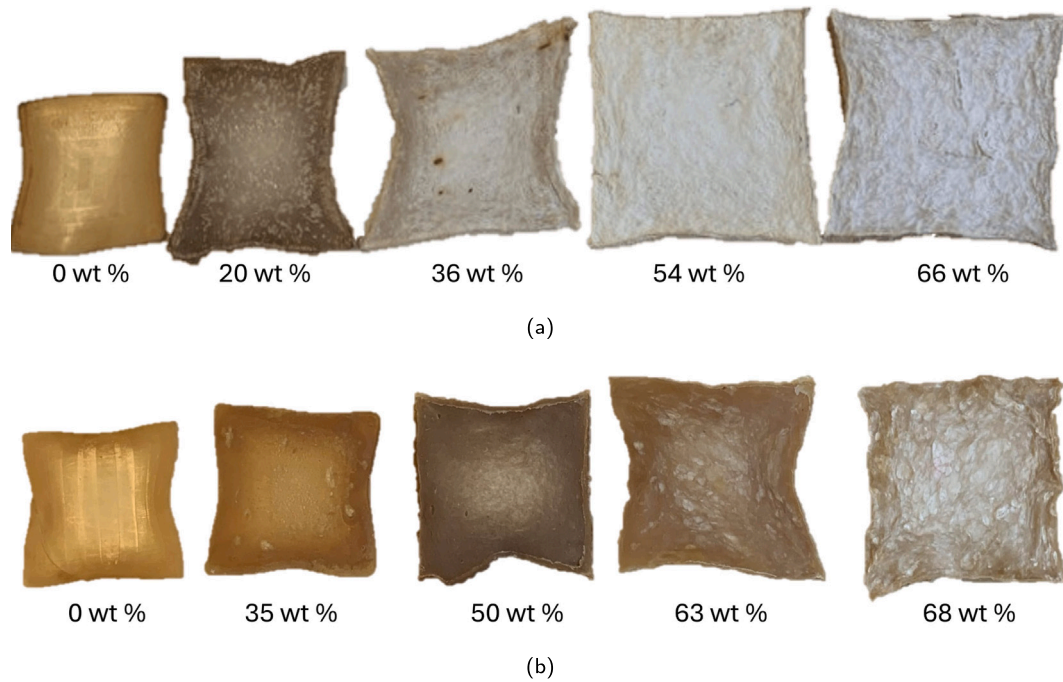


**Fig. 2.** Images of example composites ranging from 0 to approximately 70 wt% fibre content for (a) cellulose matrices reinforced with cotton flock and (b) hybrid matrices reinforced with cotton flock. In the image, reinforcement concentration increases from left to right.

where  $\epsilon_f$  is the strain in the sample (mm/mm),  $D$  is the maximum displacement (mm), and  $L$  is the original gauge length (mm). Values for Young's Modulus, strain at failure, and maximum strength were averaged over at least five measurements with uncertainties calculated as the standard error.

### 2.3.2. Bulk density analysis - Gravimetric method

The bulk density of samples was calculated as the mass divided by the total volume. RS PRO digital callipers (Corby, UK) were used to measure thicknesses. Five measurements were taken and a mean average was obtained. The cross-sectional area was obtained with ImageJ for each sample as seen in Figure S3. The density was then calculated by dividing the mass of each sample by its volume.

### 2.3.3. True density analysis- Pycnometry

Gas pycnometry was used to determine the true density of the samples. Measurements were taken with an Ultrapyc 5000 from Anton Paar (Luton, United Kingdom). Samples were pelletised into 5 mm<sup>2</sup> sizes before purging and equilibrating to 20 °C for 1 min. A flow of nitrogen at 18 psi was used on samples of approximately 10 cm<sup>3</sup> volume. Values were taken as an average over 5 runs in which variation percentage was lower than 0.1%.

### 2.3.4. X-Ray Diffraction (XRD)

X-ray studies of the samples were performed at room temperature, using Cu K $\alpha$  radiation ( $\lambda = 1.54 \text{ \AA}$ ) at 40 kV and 30 mA on a DRONEK 4-AXES Huber Diffractionstechnik (GmbH & Co. KG, Germany). The samples were mounted on a goniometer. The diffraction intensity data was collected in transmission mode. XRD data was collected with an equatorial ( $2\theta$ ) scan from  $2\theta = 8$  to  $30^\circ$ , at a scanning rate of  $0.02^\circ \text{ min}^{-1}$  and a  $2\theta$  step of  $0.2^\circ$ . The fitting method and discussion can be found in the supplementary information with Figure S4 and S5 [3,13,16,34–43]. In addition, to investigate crystallite orientation scans from  $\alpha = 0$  to  $90^\circ$  were performed at a scanning rate of  $0.02^\circ \text{ min}^{-1}$  and an  $\alpha$  step of  $0.2^\circ$ . The  $2\theta$  angle was set to  $22.4^\circ$  to probe the orientation behaviour of cellulose I crystals and hence of reinforcing fibres.

### 2.3.5. Reinforcement volume fraction analysis

The volume fraction of internal reinforcing fibres (cotton flock) was estimated using analysis of crystalline polymorphs from XRD. This was done to overcome difficulties in distinguishing the fibres from the chemically indistinct and interdiffused matrix. Firstly, the ratio of Cellulose I to Cellulose II crystalline polymorphs in cotton flock ( $R_{CF}$ ) was derived by the following equation:

$$R_{CF} = \frac{CI_{\text{Cellulose I}}}{CI_{\text{Cellulose II}}} \quad (3)$$

where  $CI_{\text{Cellulose I}}$  is the crystallinity index of Cellulose I determined as described Figures S4. The ratio of Cellulose I to Cellulose II crystalline polymorphs in each composite,  $R_{\text{Composite}}$ , is then found for all samples. As Cellulose I is only present in raw/undissolved cellulose samples it can then be assumed all Cellulose I content is present only in the undissolved reinforcing fibres [16,38]. By assuming that diffraction intensity correlates with the volume fraction of the diffracting polymorph the volume percentage of cotton flock content ( $Vol\%_{CF}$ ) can be estimated by:

$$Vol\%_{CF} = \frac{R_{\text{Composite}}}{R_{CF}} \times 100\% \quad (4)$$

### 2.3.6. Scanning Electron Microscopy (SEM)

Cross-sectional samples taken from tensile testing were first coated with a 20 nm carbon layer using Leica ACE 600 evaporative coater (Deerfield, US). Samples were then imaged using an Hitachi SU3900 SEM (Chiyoda, Japan) at 15 kV accelerating voltage and under a vacuum of 50 Pa. Images shown are from the ultra vacuum detector collecting secondary electrons and scale bars can be seen included in all images.

### 2.3.7. Optical microscopy

After fabrication, cross-sections of each sample were cut and imaged on glass slides. Images were taken in transmission mode at  $5\times$  magnification using a Leica cross-polarised light microscope (London, United Kingdom) with a Nikon D7200 digital camera (Tokyo, Japan). Multiple images were taken across the whole sample to ensure that the results were fully representative of bulk sample behaviour, though they show an example of a local region.

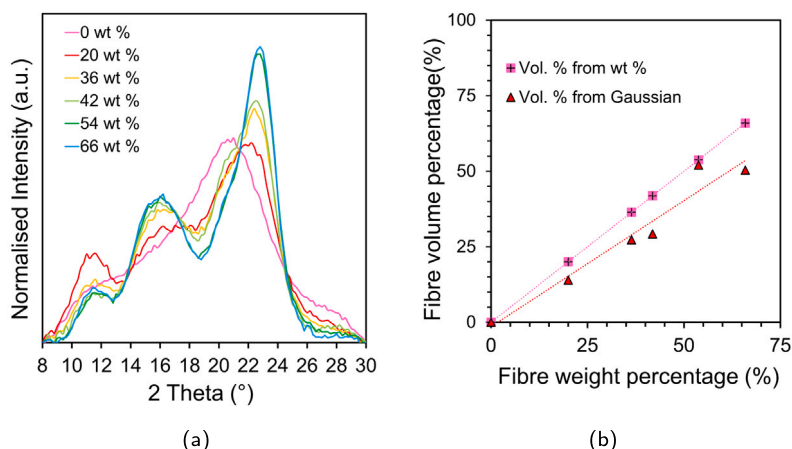


**Fig. 3.** Graphs showing (a) normalised XRD diffractograms for composite samples with cellulose matrix and cotton flock reinforcement with fibre weight percentage indicated, and (b) calculated fibre volume percentages against the fibre weight percentage. The fibre volume percentages have been calculated from Eq. (4) with gaussian peak fitting of XRD, or by assuming the fibre weight percentage is equal to its fibre volume percentage.

### 2.3.8. Flock analysis

To aid with theoretical modelling of the composite behaviours, representative samples of the reinforcing cotton flock were dispersed on glass slides, imaged, and analysed to indicate the distribution of fibre lengths, widths, and aspect ratios. Images were taken in transmission mode at  $10\times$  magnification using a Leica non-polarised light microscope (London, United Kingdom) with a Nikon D7200 digital camera (Tokyo, Japan). Multiple images were taken across five different samples and a total of more than 1000 individual fibres were counted. Fibre lengths and widths were analysed in ImageJ as shown in Figure S6. The lengths and widths were used to calculate the aspect ratio and distributions were used to generate mean, median, and modal average values as shown in Figure S7. As shown to be suitable by Virk et al., the median was used for theoretical modelling though the mean average has been used in other studies [44,45].

### 2.3.9. Acoustic insulation analysis

To demonstrate the applicability of the materials the acoustic insulation behaviours of the samples were tested. The sound transmission loss of normal incidence was measured using a BSWA impedance tube (Beijing, China) according to ASTM E2611-17. Tests were conducted from 1000–6300 Hz in a 30 mm tube (SW477). The test frequency span was 2 Hz and testing was performed at room temperature. Samples were prepared with a 30 mm diameter and care was taken to ensure the samples were snug with the interior tube surface [46].

## 3. Results and discussion

### 3.1. Morphology analysis

Morphological analysis was performed using XRD to indicate the crystalline and amorphous morphology of samples. This indicated an increasing presence of Cellulose I with increased content of undissolved fibres as shown in Fig. 3(a). These crystallinity of samples was estimated with Gaussian fittings then used to calculate the fibre volume percentages shown in Fig. 3(b). Only analysis for samples with cellulose matrices have been included as SF and cellulose crystals produce overlapping peaks in the  $2\theta$  scans and hence cannot be fitted using the same gaussian method in XRD. Discussion of this behaviour can be seen below Figures S4 and S5.

On addition of undissolved fibres, the relative size of the cellulose I peaks can be seen to increase. This can be seen in particularly in the main diffraction peak at  $22.4^\circ$  in Fig. 3a. Simultaneously, Cellulose II peaks and the central amorphous peak at  $\approx 19^\circ$  are seen to decrease

relatively. This is reflected in the estimated volume fraction of cotton fibre increasing with added cotton fibre content in Fig. 3(b).

Notably, the calculated volume fraction of cotton fibres is lower than that estimated by assuming the fibre weight percentage is equal to its fibre volume percentage. Assuming the density of the cellulose fibres and matrix are equivalent as shown in Section 3.2, this indicates that partial dissolution is occurring. This is supported by previous studies showing the concentration of the matrix solution is slightly below that of the maximum saturation concentration of the chosen solvent mixture [3]. This is also supported by the cohesive matrix-fibre interface shown in Section 3.4, indicating polymer penetration from matrix to fibre, as shown in other studies including partial dissolution [21,47,48]. As hybrid samples could not be characterised using this method, the average percentage of undissolved cotton flock was calculated as  $\%_{UCF} = \frac{Vol\%_{CF}}{Vol\%_{Weight}} \times 100\%$  where  $Vol\%$  is the volume percentage calculated from gaussian fitting or estimated as equal to the weight percentage. From this  $\%_{UCF} = 78 \pm 5\%$  which was used to estimate the  $Vol\%_{CF}$  for hybrid samples. Volume percentage is used to indicate fibre content in samples for subsequent mechanical analyses in this manuscript unless otherwise mentioned.

### 3.2. Density analysis

Inclusion of reinforcing fibres was observed to effect sample processing and the resulting sample structure. Densities of samples were measured using bulk gravimetric techniques and results can be seen in Fig. 4.

It can be seen that addition of reinforcing flock causes a reduction in sample density with both hybrid and cellulose matrices. As the cellulosic fibres have an approximately equal density to the matrices ( $1.3\text{--}1.5\text{ g cm}^{-3}$ ) [21,49], it can be assumed that the large density decrease is correlated with the presence of internal pores. This is also confirmed by the true density analysis shown in Figure S8 which showed no change in sample true density with changes in content of fibres at  $1.512 \pm 0.004\text{ g cm}^{-3}$  and  $1.498 \pm 0.002\text{ g cm}^{-3}$  for samples with pure cellulose or hybrid matrices respectively. This assumption is supported by work by Yong et al. showing density reductions to be caused by internal voiding [50]. The presence of pores is indicated by visual evidence in Section 3.4. It was found, during process optimisation, that compressing samples less during manufacture also produced lower density samples. This further indicates the density behaviour is dictated by the presence of voids. This trend is caused by the increasing viscosity of samples during mixing, as undissolved fibres are added, avoiding the collapse of voids during processing. Victoria et al. also noted reduced density due to void formation in equivalent

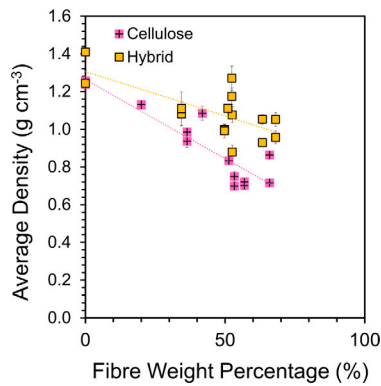


Fig. 4. Graph showing the density values of samples with linear fittings for composite samples with hybrid and cellulose matrices. The gradient of these linear fittings, as shown in Table 1, is taken to aid in later fittings of modulus theory.

Table 1

Fit parameters for a generalised linear equation,  $y = mx + c$ , for hybrid and cellulose density data as shown in Fig. 4. The larger magnitude of the negative gradient,  $c$ , for cellulose samples indicates the greater dependence of cellulose sample density on flock content.

Matrix	$c$	$m$
Cellulose	$1.26 \pm 0.05$	$-0.8 \pm 0.1$
Hybrid	$1.31 \pm 0.07$	$-0.5 \pm 0.1$

samples where solvent or solution penetration was inhibited between reinforcing fibres [15].

The cellulose samples show a larger decrease in density than the hybrid samples with addition of flock. This may be due to the reduced viscosity of SF solutions in comparison to cellulose solution (due to greater chain flexibility and/or lower molecular weights) increasing fibre penetration and reducing total void content [1,3,23]. Alternatively, the improved solvation ability of the hybrid solution utilised could dissolve more fibre content and hence cause increased void collapse [1,3,23,24]. Linear fits of the data for cellulose and hybrid samples. The results of this are shown in Table 1. These fits of sample density behaviours are utilised to estimate trends with respect to density changes in Section 3.3. It may be of future interest to replace the reinforcement with air-laid nonwoven textile waste mats as lower density reinforcement examples to reduce density further for specialised applications [18].

### 3.3. Bulk mechanical properties analysis

To test mechanical performance of samples tensile testing was performed as shown in Fig. 5. This was done to indicate the bulk behaviours of the composites and compare performance between hybrid and cellulose samples.

Fig. 5(a) and (b) show the stress–strain curves for cellulose samples. It can be seen that samples with higher fibre content did not show brittle failure, as indicated by steep drop in stress after failure. This is caused by the fibre-pullout failure mechanism causing a more gradual reduction in stress upon failure. Variation in this mechanism leads to larger standard error in these samples, though uncertainty was already pronounced due to sample warp and variation in lab-scale fabrication potentially impacting local fibre alignment. It is also notable that the maximum stress achieved with cellulose samples was lower than that of the hybrid samples. This is primarily due to the presence of significant void content discussed in Section 3.2, and the inferior fibre-matrix bonding seen in cellulose samples with insufficient matrix causing fibre pullout. Secondly, additional processing time could impact fibre

quality due to heat or solvent induced degradation and reduce this value.

As shown in Fig. 5(c), both sets of composite samples showed comparable increase in the specific Young's modulus with increases in the fibre volume percentage. As trends in specific modulus agree, within uncertainty, for both hybrid and cellulose matrices it is indicated that the modulus of samples is primarily controlled by the volume percentage of the reinforcing fibres. In support of this, it was shown by Mohammadi et al. that aligned SF or cellulose fibres can improve modulus beyond those seen in unaligned examples [1,14]. This holds true as long as the supporting matrix is of sufficient volume and interfacial adhesion to transfer composite stress to the internal fibres. Deviation from the trend can be seen at maximum content of fibre volume percentage as insufficient matrix is seen in this sample to provide a cohesive composite [51]. The maximum volume percentage achieved was higher than that of typical randomly reinforced composite samples ( $V_f = 0.1 - 0.3$ ) [52]. This may be due to reinforcing fibre flexibility, or dissolution which is not considered in the optimal cases [3,52].

It can also be noted for these samples that a negative correlation is broadly observed between sample density and Young's modulus. This breaks from typical convention, as shown in Figure S2, and arises due to the reinforcing fibre both encouraging reduced sample density and increasing sample modulus [15,51]. This simultaneous effect improves samples stiffness while reducing density. This arises due to the described reinforcing behaviour of fibre inclusion occurring alongside cavity formation described in Section 3.2. This could indicate a use for these composites in low density applications.

The hybrid composites are able to form composites with higher volume percentages of fibres due to reduced viscosity and increased saturation concentration of the hybrid solution. This allows for effective inclusion of higher quantities of fibres and hence a greater maximum modulus. Secondly, the hybrid matrix exhibits a greatly improved maximum strain at failure performance at optimal fibre loading, as shown in Fig. 5(e). This may be due to improved matrix extensibility as a result of time-dependent relaxations incurring viscoelastic behaviour in the polymer blend [13,14]. In these samples sacrificial bonds allow for localised failure and total network relaxation which mimics behaviours seen in high performance natural double networks [13,53–56]. This allows fibres to be loaded more effectively and could lead to the dramatic increase in failure stress shown in these samples. The distinct peak in max strength and strain occurs between 42–55 fibre vol% in hybrid samples.

To validate modelling, experimental results can then be plotted against the theoretical predictions of modulus by standard composite mixing models. The modified rule of mixing was altered to model the modulus of the composite ( $E_C$ ) while considering the void content with the following equation [44,45,51]:

$$E_C = (\eta_O \eta_L E_f f_i + (1 - f_i) E_m) \times \frac{\rho_i}{\rho_{matrix}} \quad (5)$$

where  $E$  is the modulus of the composite, fibre, or matrix respectively (GPa);  $\eta_O$  is the Krenchel orientation factor;  $\eta_L$  is the Cox shear lag factor;  $f_i$  is the fibre volume fraction corresponding to sample  $i$ ; and  $\rho$  is the density of the pure matrix or the composite respectively. As discussed in Figure S10, the density term is taken to represent the presence of voids not contributing to stress loading in extension. The reinforcement was modelled as randomly oriented in plane ( $\eta_O = 3/8$ ). The aspect ratio of fibres was found, in Section 2.3.8, to be 13.2. This provides a reinforcing efficiency of 87 % based on the Cox Shear lag factor as shown in Figure S9. The full derivation of the equation and description of all factors can be found with Figure S10 including data and fitting for cellulose samples [44,45,51,57–59]. The moduli of hybrid samples is fitted against Eq. (5) in Fig. 6.

It can be seen from Fig. 6 that experimental results agree with theoretical fittings, within uncertainties, until composite failure is seen due to insufficient matrix content. This confirms the validity of the

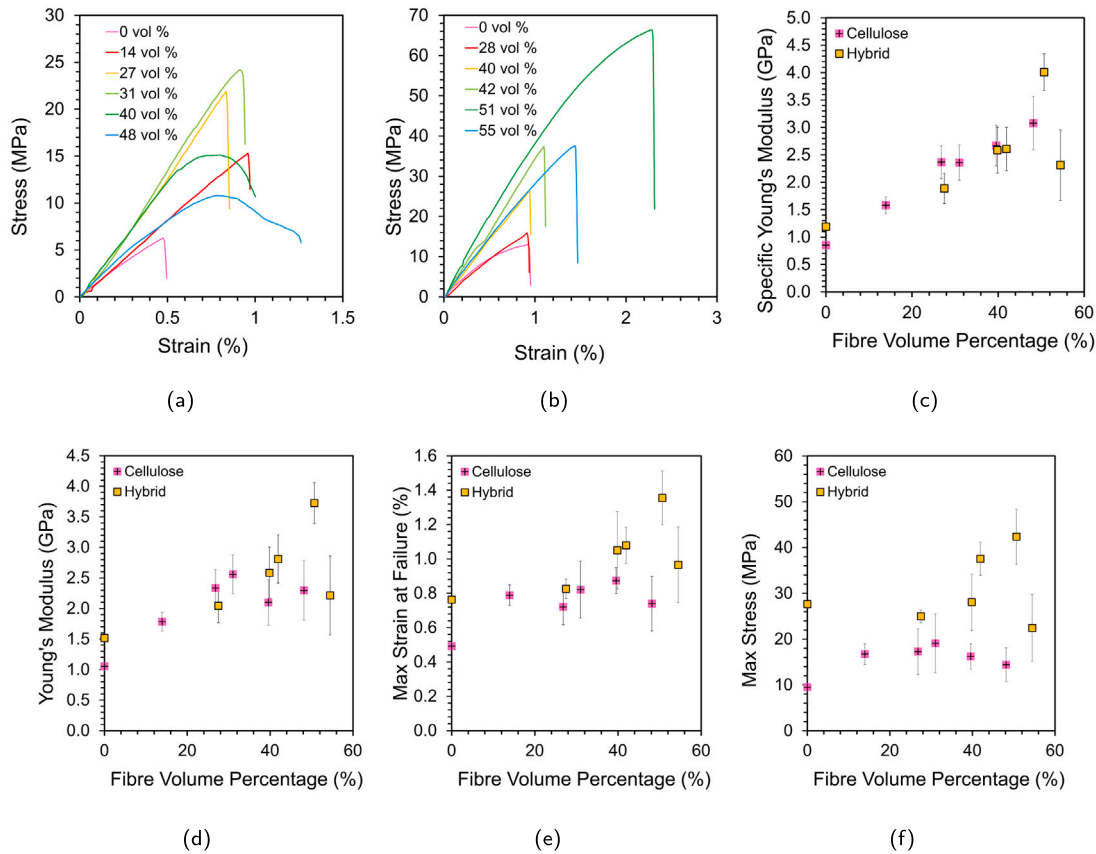


**Fig. 5.** Graphs showing example representative stress–strain curves for tensile testing of (a) cellulose samples, and (b) hybrid samples with extracted average data showing (c) the specific Young's Modulus, (d) the Young's Modulus, (e) max strain at failure, and (f) max strength. The numbers included in the legend of the example stress–strain curves indicate the volume percentage of included flock reinforcement for each sample.

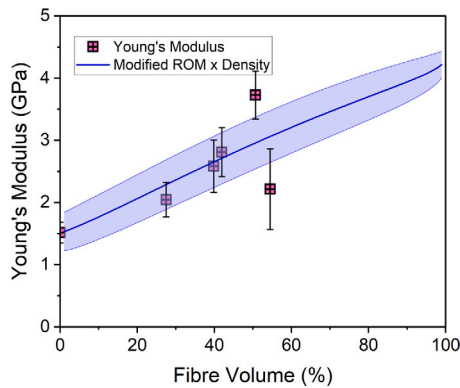


**Fig. 6.** Graph showing the tensile modulus against the fibre volume percentage for all experimentally measured hybrid samples. The solid line shows the modified rule of mixtures prediction included Cox, Krenchel, and density fitting parameters. Errors shown with the shaded region are calculated using error propagation.

model described in Eq. (5) and implies the tunability of the field of composites for multiple applications requiring varied moduli. Though sufficient, the model may be further improved by additional factors to account for the following assumptions which may not always hold true for the composites in question:

1. Fibres are linear and unbent
2. Fibre-matrix interfacial adhesion is perfect
3. The fibres and matrix are under uniform tensile strain

To confirm the system optimum with fibre volume percentage for samples with hybrid matrices several samples were prepared with an optimal fibre content of 48 vol% and tensile tested. This confirmed the maximum in sample modulus at  $3.3 \pm 0.3$  GPa, and indicated bulk anisotropy in samples by testing samples at 0, 45, and 90° directions. This can be seen in Figure S11. Local isotropy was also tested using XRD and confirmed that samples showed local directionality on the sub-mm lengthscale, as shown in Figure S12. This was indicated by orientation in an alpha scan, which tests on the mm length scale of the beam thickness, and so shows that fibres remain locally oriented in the composite.

The mechanical performance of these materials indicates a host of promising applications. For example, the sample modulus is within the range seen for cancellous bone (0.05–5 GPa) [24,60]. This, alongside literature evidence of biocompatibility, shows that these materials could be used to create biomimetic materials for wound healing applications [61].

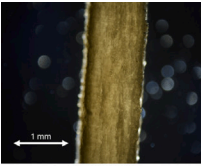
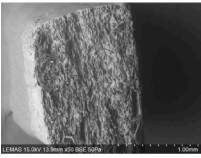
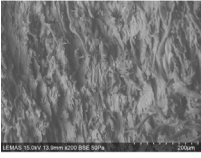
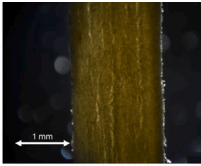
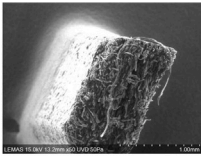
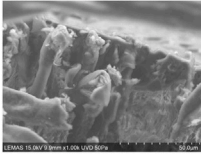
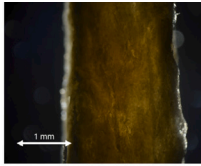
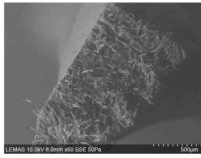
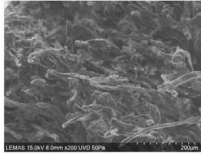
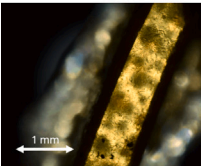
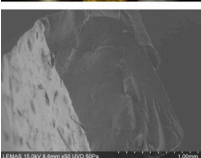
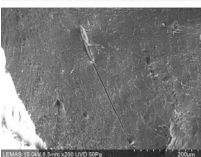
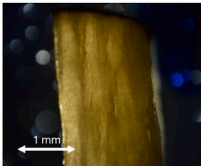
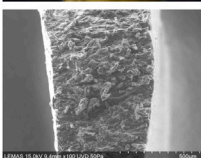
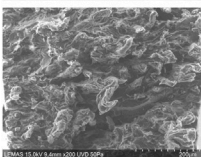
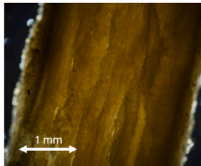
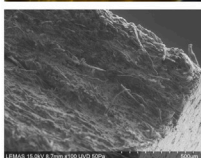
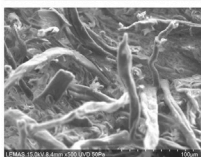
### 3.4. Failure analysis - Sample imaging

After testing, sample failure mechanisms and structures were analysed by imaging with both polarised optical microscopy and SEM. Polarised optical microscopy was performed on thin cross sections cut from samples while SEM was performed directly on the failure cross sections of tensile tested samples. Images of the samples can be seen in Table 2.

Light microscopy in Table 2 shows increasing evidence of voids and laminar gaps forming as fibre content increases. This is supported by the increased laminar separation in SEM images of 50% fibre volume cellulose samples. This coincides also with increased fibre pullout in



**Table 2**  
Images of composite cross sections for cellulose and hybrid samples in polarised optical microscopy and SEM. Samples of various fibre volume percentages shown at different magnifications.

Cellulose Matrix		
25 %	40 %	50 %
  	  	  
Hybrid Matrix		
30 %	40 %	55 %
  	  	  

these samples, causing the distinct stress–strain curves shown in Section 3.3 (a). It appears that fibre matrix interfaces are more smoothly integrated at 40% fibre volume in both matrices than in the upper extremes, though superior interfacial adhesion is seen in the hybrid matrix. This confirms discussion of the hybrid matrix’s superior processing power at higher fibre concentrations as discussed in Section 3.3.

In hybrid samples, the increased dissolving ability is clearly demonstrated by the lack of fibres at the surface of 30% fibre volume sample. This instead demonstrates a brittle fracture surface with a chevroned fracture surface and smooth surfaces along crystallographic planes [62]. This indicates that further research into the fibre volume analysis could be of interest for these complex novel materials to improve the estimations used in this study. 40 and 50% fibre volume samples show similar trends to cellulose samples with increasing fibre pull out and interlaminar failure in highly reinforced samples. It can be seen that at 40% fibre volume good matrix-fibre adhesion is seen and fibres pull-out appears to be limited, which indicates proper fibre loading [51,63].

### 3.5. Acoustic insulation analysis

To indicate the potential application of these materials in non-load bearing acoustic insulation capacities the acoustic insulation performance was tested with respect to matrix and reinforcing flock. The sound transmission loss performance can be seen in Fig. 7 with the average transmission loss across the tested frequencies given in Table 3.

Fig. 7 and Table 3 show that hybrid samples achieved a greater average acoustic transmission loss ( $47 \pm 7$  dB) compared to that of cellulose samples ( $29 \pm 4$  dB), again indicating their improved performance. An increase in average transmission loss was seen increasing fibre content for samples with both cellulose and hybrid matrices. This indicates an improved acoustic insulation performance. This behaviour is mediated by sound wave interactions with material micropores and macrostructure [20]. Acoustic insulation can be aided (in porous materials) by air molecules vibrating to transform acoustic vibrations into viscous and thermal energy, or (in fibrous materials) energy being transformed into fibre vibrations [20]. In these composites, closed-cell cavities may be formed by interstices of fibres where matrix was unable to enter during



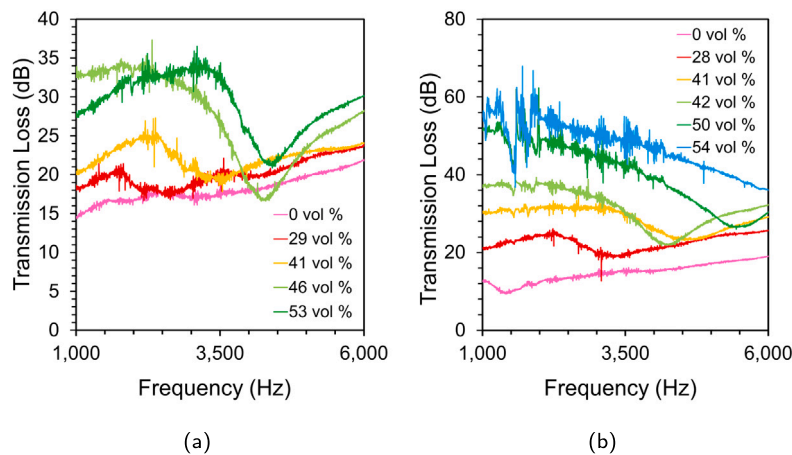


**Fig. 7.** Acoustic transmission loss plotted against frequency for both (a) cellulose matrix, and (b) hybrid matrix samples. The numbers included in the legend indicate the volume percentage of included flock reinforcement for each sample.

**Table 3**

Average values and standard deviation derived from acoustic transmission loss graphs for both cellulose matrix, and hybrid matrix samples. For clarity, transmission loss has been abbreviated to TL in the table below.

Cellulose	Fibre vol (%)	0%	29%	41%	46%	53%	
	Average TL (dB)	18 ± 2	20 ± 2	22 ± 2	28 ± 5	29 ± 4	
Hybrid	Fibre vol (%)	0%	28%	41%	42%	50%	54%
	Average TL (dB)	15 ± 3	23 ± 2	29 ± 3	32 ± 5	40 ± 8	47 ± 7

preparation [20]. The increasing addition of fibres may greatly improve scattering by introducing interfaces between fibres, matrix, and cavities and hence to improve acoustic insulation. The improved performance at low frequencies is comparable to work by Sui et al. on honeycomb acoustic metamaterials [64]. Multiple reflections between interfaces was proposed to encourage standing waves which greatly improved the transmission loss [64]. Sample acoustic performance was superior to standard single layer building materials (plywood, aerated concrete, laminated glass, and rock wool) which largely showed transmission loss below 25 dB when below 1000 Hz [65,66].

Notably, the performance of samples with hybrid matrices was superior to samples with cellulose matrices. This may be related to increased sample density, as seen in Fig. 4, which is shown to increase acoustic insulation in accordance with the mass law [67]. Though promising, these results should be considered as only preliminary evidence of performance as it is likely surface behaviours affected the acoustic performance which would be magnified by the use of relatively thin samples in this case [68]. The effect of fibre content on pore size and surface roughness should be considered in future studies more primarily focused on acoustic performance.

Dips in the transmission loss can be seen in Fig. 7(a) and (b) which occur at higher frequencies as the fibre content is increased. This is likely the samples critical valley, at which the bending wavelength matches the acoustic wavelength [67]. This allows more efficient transfer of sound wave energy across the sample. The frequency of the critical valley increases with flock content and likely corresponds to the bending wavelength of the material decreasing with its modulus change, as shown in Fig. 5(d). This indicates the tunability of this material for selective insulation over certain frequencies.

Fig. 7 offers an initial look at the acoustic performance of these materials and indicates the fruitful application of these materials. It can be observed that the maximum transmission loss performance ( $\approx 60$  dB) exceeds the typical standard for internal interior soundproofing between rooms (45 dB) though the performance must be compared over relevant frequencies [69]. This is achieved without significant mass increase, contrary to the typical mass law, and so offers the potential for application as a lightweight, sustainable, insulative material [19,67,69].

Further sound absorption studies would allow an improved understanding of this performance in more varied applications [46]. To further optimise these materials, future studies could seek to combine these novel materials with other techniques to maximise performance. Liu et al. showed effective sound absorption in honeycomb sandwich composites with woven skin structures [68]. A noise reduction coefficient of 0.670 was achieved with a double layered structure to optimise sound absorption induced by thermofriction between the air and fabric, and cavity resonance [68]. The noise reduction coefficient indicates the ability of the partition, at specific mid-range frequencies to reflect noise. It ranges from 0 (complete reflection) to 1 (no reflection). Combining structural design techniques with our new material could improve sound absorption and transmission loss over a broad range of frequencies with promising applications [19,70]. The mechanical and acoustic properties could enable uses as a sustainable building material for interior decoration [19,28]. Due to sample flammability, to achieve these applications flame retardancy treatments should be a priority of focus for future study [71]. Surface treatments could improve sample fire retardancy for wider application [72].

#### 4. Conclusions

This study has demonstrated the feasibility of a novel isotropically reinforced short-fibre biopolymer composite and confirmed the effectiveness of an optimised hybrid cellulose/silk fibroin matrix in reinforced composites. The results highlight the importance of innovative biopolymer hybrid blends in developing high-performance, tunable biomaterials for diverse applications.

Solutions of pure cellulose and a 10:90 SF/cellulose hybrid blend were isotropically reinforced with cotton flock through mixing, coagulation, washing, and drying, yielding composite samples with an optimal balance of low density and mechanical properties. The modulus increased with fibre content, while density decreased. Notably, the modulus trends overlapped for cellulose and silk fibroin samples, indicating that tensile modulus was governed primarily by flock content rather than the matrix. However, the hybrid matrix allowed processing with higher flock content and exhibited optima in maximum strength

and strain at failure. Additionally, the hybrid matrix demonstrated improved extensibility and interfacial adhesion, enhancing stress transfer to fibres and overall sample strength. Experimental results aligned well with a theoretical rule of mixtures incorporating Cox shear lag, Krenchel orientation, and density factors, suggesting the model's potential for predicting tunable composites for acoustic or biomedical applications.

Further investigation into their practical performance and end-of-life behaviour—such as degradation studies and life-cycle analysis—could better assess their environmental sustainability and broaden their applicability. This study indicates the potential benefits of using hybrid biopolymer blends in biocomposite creation and provides scope for further study into differing blends, reinforcement types, and applications of this novel set of materials. Future study should test the scalability of the sample production and directly test sample performance in non-load bearing acoustic building applications.

## Abbreviations

The following abbreviations are used in this manuscript:

SF	Silk Fibroin
XRD	X-ray Diffraction
SEM	Scanning Electron Microscopy
EMimAc	1-ethyl-3-methylimidazolium acetate
DMSO	Dimethyl Sulfoxide
ROM	Rule of mixing

## CRediT authorship contribution statement

**James A. King:** Writing – original draft, Validation, Methodology, Investigation, Formal analysis, Data curation, Conceptualization. **Peter J. Hine:** Writing – review & editing, Validation, Supervision, Resources. **Daniel L. Baker:** Writing – review & editing, Validation, Supervision, Resources. **Yu Shi:** Writing – review & editing, Validation, Resources. **Xiaoling Liu:** Writing – review & editing, Validation, Resources. **Jiawen Lu:** Writing – review & editing, Validation, Data curation. **Saihua Li:** Writing – review & editing, Validation, Data curation. **Xiaoye Cong:** Writing – review & editing, Validation. **Michael E. Ries:** Writing – review & editing, Validation, Supervision, Resources, Investigation.

## Funding

James King was supported by the EPSRC CDT in Soft Matter for Formulation and Industrial Innovation, “SOFI<sup>2</sup>”, (EP/S023631/1). This research also received funding from the European Union's Horizon 2020 research and innovation programme under the Marie Skłodowska-Curie grant agreement No 101007429 (INTAKE).

## Declaration of competing interest

The authors declare the following financial interests/personal relationships which may be considered as potential competing interests: The authors declare that they have no known competing financial interests or personal relationships that could have appeared to influence the work reported in this paper.

## Acknowledgements

With many thanks to my supervisory team of Mike, Peter, and Dan for their constant patience and kindness. Scanning electron microscopy imaging was performed by Stuart Micklethwaite, at the Leeds Electron Microscopy And Spectroscopy Centre. I would also like to thank Professor Yu Shi for his enthusiasm and support. Lastly, thank you to Prof. Xiaoling Liu for hosting my research at the University of Nottingham, Ningbo and to Jiawen, Crystal, Xiaoye, and the other team members who made my stay there so enjoyable.

## Appendix A. Supplementary data

Supplementary material related to this article can be found online at <https://doi.org/10.1016/j.compositesa.2025.109459>.

## Data availability

All data needed to evaluate the conclusions in the paper are present in the paper and/or the Supplementary Materials. In addition, the data associated with this paper are openly available from the University of Leeds Data Repository at <https://doi.org/10.5518/1751>.

## References

- [1] Kostag M, Jedvert K, El Seoud OA. Engineering of sustainable biomaterial composites from cellulose and silk fibroin: Fundamentals and applications. *Int J Biol Macromol* 2021;167:687–718. <http://dx.doi.org/10.1016/j.ijbiomac.2020.11.151>.
- [2] French AD. Glucose, not cellobiose, is the repeating unit of cellulose and why that is important. *Cellulose* 2017;24(11):4605–9. <http://dx.doi.org/10.1007/s10570-017-1450-3>.
- [3] King JA, Hine PJ, Baker DL, Ries ME. Understanding the dissolution of cellulose and silk fibroin in 1-ethyl-3-methylimidazolium acetate and dimethyl sulphoxide for application in hybrid films. *Materials* 2024;17(21):5262. <http://dx.doi.org/10.3390/ma17215262>, URL <https://www.mdpi.com/1996-1944/17/21/5262>.
- [4] Li J, Nawaz H, Wu J, Zhang J, Wan J, Mi Q, Yu J, Zhang J. All-cellulose composites based on the self-reinforced effect. *Compos Commun* 2018;9(April):42–53. <http://dx.doi.org/10.1016/j.coco.2018.04.008>.
- [5] Holland C, Numata K, Rnjak-Kovacina J, Seib FP. The biomedical use of silk: Past, present, future. *Adv Healthc Mater* 2019;8(1). <http://dx.doi.org/10.1002/adhm.201800465>.
- [6] El Seoud OA, Jedvert K, Kostag M, Possidonio S. Cellulose, chitin and silk: the cornerstones of green composites. *Emergent Mater* 2021;5:785–810. <http://dx.doi.org/10.1007/s42247-021-00308-0>.
- [7] Noishiki Y, Nishiyama Y, Wada M, Kuga S, Magoshi J. Mechanical properties of silk fibroin-microcrystalline cellulose composite films. *J Appl Polym Sci* 2002;86(13):3425–9. <http://dx.doi.org/10.1002/app.11370>.
- [8] Blessing B, Trout C, Morales A, Rybacki K, Love SA, Lamoureux G, O'malley SM, Hu X, Salas-De la Cruz D. The impact of composition and morphology on ionic conductivity of silk/cellulose bio-composites fabricated from ionic liquid and varying percentages of coagulation agents. *Int J Mol Sci* 2020;21(13):1–23. <http://dx.doi.org/10.3390/ijms21134695>.
- [9] Wang K, Ma Q, Zhang YM, Han GT, Qu CX, Wang SD. Preparation of bacterial cellulose/silk fibroin double-network hydrogel with high mechanical strength and biocompatibility for artificial cartilage. *Cellulose* 2020;27(4):1845–52. <http://dx.doi.org/10.1007/s10570-019-02869-0>.
- [10] Guzman-Puyol S, Heredia-Guerrero JA, Ceseracciu L, Hajiali H, Canale C, Scarpellini A, Cingolani R, Bayer IS, Athanassiou A, Mele E. Low-cost and effective fabrication of biocompatible nanofibers from silk and cellulose-rich materials. *ACS Biomater Sci Eng* 2016;2(4):526–34. <http://dx.doi.org/10.1021/acsbomaterials.5b00500>.
- [11] Tian D, Li T, Zhang R, Wu Q, Chen T, Sun P, Ramamoorthy A. Conformations and intermolecular interactions in cellulose/silk fibroin blend films: A solid-state NMR perspective. *J Phys Chem B* 2017;121(25):6108–16. <http://dx.doi.org/10.1021/acs.jpcc.7b02838>.
- [12] DeFrates K, Markiewicz T, Callaway K, Xue Y, Stanton J, Salas-de la Cruz D, Hu X. Structure–property relationships of Thai silk–microcrystalline cellulose biocomposite materials fabricated from ionic liquid. *Int J Biol Macromol* 2017;104:919–28. <http://dx.doi.org/10.1016/j.ijbiomac.2017.06.103>.
- [13] King JA, Hine PJ, Baker DL, Creswick M, Ries ME. Hybrid biocomposites: From molecular behaviour to material properties in silk fibroin/cellulose films. *Int J Biol Macromol* 2025;145931. <http://dx.doi.org/10.1016/j.ijbiomac.2025.145931>, URL <https://www.sciencedirect.com/science/article/pii/S0141813025064864>.
- [14] Mohammadi P, Aranko AS, Landowski CP, Ikkala O, Jaudzems K, Wagermaier W, Linder MB. Biomimetic composites with enhanced toughening using silk-inspired triblock proteins and aligned nanocellulose reinforcements. *Sci Adv* 2019;5(9). <http://dx.doi.org/10.1126/sciadv.aaw2541>.
- [15] Victoria A, Edward Ries M, John Hine P. Use of interleaved films to enhance the properties of all-cellulose composites. *Compos A* 2022;160(March):107062. <http://dx.doi.org/10.1016/j.compositesa.2022.107062>.
- [16] Gupta KM, Jiang J. Cellulose dissolution and regeneration in ionic liquids: A computational perspective. *Chem Eng Sci* 2015;121:180–9. <http://dx.doi.org/10.1016/j.ces.2014.07.025>.
- [17] Ciobanu L. Development of 3D knitted fabrics for advanced composite materials. In: *Advances in composite materials - ecodeign and analysis*. InTech; 2011, p. 161–90. <http://dx.doi.org/10.5772/14876>, URL <https://api.semanticscholar.org/CorpusID:136557679>.

- [18] Hjelm A, Skrifvars M, Khalili P. Short fiber composites from postconsumer textile waste and their suitability in packaging applications. *Heliyon* 2025;11(3):e42335. <http://dx.doi.org/10.1016/j.heliyon.2025.e42335>.
- [19] Asdrubali F, D'Alessandro F, Schiavoni S. A review of unconventional sustainable building insulation materials. *Sustain Mater Technol* 2015;4(2015):1–17. <http://dx.doi.org/10.1016/j.susmat.2015.05.002>.
- [20] Berardi U, Iannace G. Acoustic characterization of natural fibers for sound absorption applications. *Build Environ* 2015;94(July):840–52. <http://dx.doi.org/10.1016/j.buildenv.2015.05.029>.
- [21] Victoria A, Hine PJ, Ward K, Ries ME. Design of experiments in the optimization of all-cellulose composites. *Cellulose* 2023;30(17):11013–39. <http://dx.doi.org/10.1007/s10570-023-05535-8>.
- [22] Asdrubali F. The role of life cycle assessment (LCA) in the design of sustainable buildings: Thermal and sound insulating materials. In: 8th European conference on noise control 2009, EUROISE 2009 - proceedings of the institute of acoustics. 2009;vol. 31. PART 3.
- [23] Zhang X, Ries ME, Hine PJ. Time-temperature superposition of the dissolution of silk fibers in the ionic liquid 1-ethyl-3-methylimidazolium acetate. *Biomacromolecules* 2021;22(3):1091–101. <http://dx.doi.org/10.1021/acs.biomac.0c01467>.
- [24] King JA, Zhang X, Ries ME. The formation of all-silk composites and time-temperature superposition. *Materials* 2023;16(10). <http://dx.doi.org/10.3390/ma16103804>.
- [25] Azimi B, Maleki H, Gigante V, Bagherzadeh R, Mezzetta A, Milazzo M, Guazzelli L, Cinelli P, Lazzeri A, Danti S. Cellulose-based fiber spinning processes using ionic liquids. *Cellulose*. vol. 29, Springer Netherlands; 2022, p. 3079–129. <http://dx.doi.org/10.1007/s10570-022-04473-1>.
- [26] Xi Y, Zhang L, Tian Y, Song J, Ma J, Wang Z. Rapid dissolution of cellulose in an AlCl<sub>3</sub>/ZnCl<sub>2</sub> aqueous system at room temperature and its versatile adaptability in functional materials. *Green Chem* 2022;24(2):885–97. <http://dx.doi.org/10.1039/d1gc03918k>.
- [27] Li X, Li H, You T, Chen X, Ramaswamy S, Wu YY, Xu F. Enhanced dissolution of cotton cellulose in 1-allyl-3-methylimidazolium chloride by the addition of metal chlorides. *ACS Sustain Chem Eng* 2019;7(23):19176–84. <http://dx.doi.org/10.1021/acssuschemeng.9b05159>.
- [28] Cianci C, Chelazzi D, Poggi G, Modi F, Giorgi R, Laurati M. Hybrid fibroin-nanocellulose composites for the consolidation of aged and historical silk. *Colloids Surfaces A* 2022;634(November 2021):127944. <http://dx.doi.org/10.1016/j.colsurfa.2021.127944>.
- [29] Chen ZJ, Zhang Y, Zheng L, Zhang H, Shi HH, Zhang XC, Liu B. Mineralized self-assembled silk fibroin/cellulose interpenetrating network aerogel for bone tissue engineering. *Mater Sci Eng C* 2021;134(November 2021):112549. <http://dx.doi.org/10.1016/j.msec.2021.112549>.
- [30] Eivazzadeh-Keihan R, Ahmadpour F, Aliabadi HAM, Radinekiyan F, Maleki A, Madanchi H, Mahdavi M, Shalan AE, Lanceros-Méndez S. Pectin-cellulose hydrogel, silk fibroin and magnesium hydroxide nanoparticles hybrid nanocomposites for biomedical applications. *Int J Biol Macromol* 2021;192(September):7–15. <http://dx.doi.org/10.1016/j.ijbiomac.2021.09.099>.
- [31] Tomimatsu Y, Suetsugu H, Yoshimura Y, Shimizu A. The solubility of cellulose in binary mixtures of ionic liquids and dimethyl sulfoxide: Influence of the anion. *J Mol Liq* 2019;279:120–6. <http://dx.doi.org/10.1016/j.jmolliq.2019.01.093>.
- [32] Guan J, Porter D, Vollrath F. Thermally induced changes in dynamic mechanical properties of native silks. *Biomacromolecules* 2013;14(3):930–7. <http://dx.doi.org/10.1021/bm400012k>.
- [33] Timoshenko S. *Strength of materials*. 3rd ed.. Princeton: Van Nostrand; 1956.
- [34] Park S, Baker JO, Himmel ME, Parilla PA, Johnson DK. Cellulose crystallinity index: measurement techniques and their impact on interpreting cellulase performance. *Biotechnol Biofuels* 2010;3. <http://dx.doi.org/10.1186/1754-6834-3-10>.
- [35] French AD. Increment in evolution of cellulose crystallinity analysis. 2020. <http://dx.doi.org/10.1007/s10570-020-03172-z>.
- [36] French AD. Idealized powder diffraction patterns for cellulose polymorphs. *Cellulose* 2014;21(2):885–96. <http://dx.doi.org/10.1007/s10570-013-0030-4>.
- [37] Hawkins JE. *Analysis of the dissolution behaviour of flax based yarn in an ionic liquid* [Ph.D. thesis], University of Leeds; 2021.
- [38] Verma C, Mishra A, Chauhan S, Verma P, Srivastava V, Quraishi MA, Ebenso EE. Dissolution of cellulose in ionic liquids and their mixed cosolvents: A review. *Sustain Chem Pharm* 2019;13(July):100162. <http://dx.doi.org/10.1016/j.scp.2019.100162>.
- [39] Segal L, Creely JJ, Martin AE, Conrad CM. An empirical method for estimating the degree of crystallinity of native cellulose using the X-Ray diffractometer. *Text Res J* 1959;29(10):786–94. <http://dx.doi.org/10.1177/004051755902901003>.
- [40] Thygesen A, Oddershede J, Lilholt H, Thomsen AB, Ståhl K. On the determination of crystallinity and cellulose content in plant fibres. *Cellulose* 2005;12(6):563–76. <http://dx.doi.org/10.1007/s10570-005-9001-8>.
- [41] Ahvenainen P, Kontro I, Svedström K. Comparison of sample crystallinity determination methods by X-ray diffraction for challenging cellulose I materials. *Cellulose* 2016;23(2):1073–86. <http://dx.doi.org/10.1007/s10570-016-0881-6>.
- [42] Zhao Q, Yam RC, Zhang B, Yang Y, Cheng X, Li RK. Novel all-cellulose eco-composites prepared in ionic liquids. *Cellulose* 2009;16(2):217–26. <http://dx.doi.org/10.1007/s10570-008-9251-3>.
- [43] Lu Q, Hu X, Wang X, Kluge JA, Lu S, Cebe P, Kaplan DL. Water-insoluble silk films with silk I structure. *Acta Biomater* 2010;6(4):1380–7. <http://dx.doi.org/10.1016/j.actbio.2009.10.041>.
- [44] Virk AS, Hall W, Summerscales J. Modulus and strength prediction for natural fibre composites. In: *Materials science and technology* (United Kingdom). vol. 28, Maney Publishing; 2012, p. 864–71. <http://dx.doi.org/10.1179/1743284712Y.0000000022>.
- [45] Hine P, Parveen B, Brands D, Caton-Rose F. Validation of the modified rule of mixtures using a combination of fibre orientation and fibre length measurements. *Compos A* 2014;64:70–8. <http://dx.doi.org/10.1016/j.compositesa.2014.04.017>.
- [46] Doutres O, Salissou Y, Atalla N, Panneton R. Evaluation of the acoustic and non-acoustic properties of sound absorbing materials using a three-microphone impedance tube. 2010. <http://dx.doi.org/10.1016/j.apacoust.2010.01.007>.
- [47] Liang Y, Hawkins JE, Ries ME, Hine PJ. Dissolution of cotton by 1-ethyl-3-methylimidazolium acetate studied with time-temperature superposition for three different fibre arrangements. *Cellulose* 2021;28(2):715–27. <http://dx.doi.org/10.1007/s10570-020-03576-x>.
- [48] Huber T, Pang S, Staiger MP. All-cellulose composite laminates. *Compos A* 2012;43(10):1738–45. <http://dx.doi.org/10.1016/j.compositesa.2012.04.017>.
- [49] Seki Y, Selli F, Erdoğan ÜH, Atagür M, Seydibeyoğlu MÖ. A review on alternative raw materials for sustainable production: novel plant fibers. *Cellulose* 2022;29(9):4877–918. <http://dx.doi.org/10.1007/s10570-022-04597-4>.
- [50] Yong L, Jian L, Xian L, Bei W. Test and analysis of the porosity of cotton fiber assembly. *J Eng Fibers Fabr* 2021;16. <http://dx.doi.org/10.1177/15589250211024225>.
- [51] Hull D, Clyne W. *An introduction to composite materials*. 2nd ed.. Cambridge: Cambridge University Press; 1996.
- [52] Summerscales J. *Composites design and manufacture module*. 2025, URL <http://lists.lib.plymouth.ac.uk/lists/15D82EF9-06E6-A71D-1544-EE8162EE9DDA.html#section-17E16A67-C278-4486-9284-4440D67327B0>.
- [53] Nakajima T. Generalization of the sacrificial bond principle for gel and elastomer toughening. *Polym J* 2017;49(6):477–85. <http://dx.doi.org/10.1038/pj.2017.12>.
- [54] Nam S, Hu KH, Butte MJ, Chaudhuri O. Strain-enhanced stress relaxation impacts nonlinear elasticity in collagen gels. *Proc Natl Acad Sci USA* 2016;113(20):5492–7. <http://dx.doi.org/10.1073/pnas.1523906113>.
- [55] Chen S, Brodersz CP, Markovich T, MacKintosh FC. Nonlinear stress relaxation of transiently crosslinked biopolymer networks. *Phys Rev E* 2021;104(3):1–14. <http://dx.doi.org/10.1103/PhysRevE.104.034418>, arXiv:2104.11868.
- [56] Mulla Y, MacKintosh FC, Koenderink GH. Origin of slow stress relaxation in the cytoskeleton. *Phys Rev Lett* 2019;122(21):218102. <http://dx.doi.org/10.1103/PhysRevLett.122.218102>, arXiv:1810.08165.
- [57] Chichane A, Boujmal R, El Barkany A. Towards a green & ecological revolution: Review of natural reinforcing bio-composites and bio-hybrid composites. 2024. <http://dx.doi.org/10.1177/09673911241226578>.
- [58] Cox HL. The elasticity and strength of paper and other fibrous materials. *Br J Appl Phys* 1952;3(3):72–9. <http://dx.doi.org/10.1088/0508-3443/3/3/302>.
- [59] Krenchel H. *Fibre reinforcement : theoretical and practical investigations of the elasticity and strength of fibre-reinforced materials*. Copenhagen: Akademisk Forlag; 1964, URL <https://lib.ugent.be/catalog/rug01:001280222>.
- [60] Chen J, Zhuang A, Shao H, Hu X, Zhang Y. Robust silk fibroin/bacterial cellulose nanoribbon composite scaffolds with radial lamellae and intercalation structure for bone regeneration. *J Mater Chem B* 2017;5(20):3640–50. <http://dx.doi.org/10.1039/c7tb00485k>.
- [61] Lee JM. The fixation effect of a silk fibroin-bacterial cellulose composite plate in segmental defects of the zygomatic arch: An experimental study. *JAMA Otolaryngol-Head Neck Surg* 2013;139(6):629. <http://dx.doi.org/10.1001/jamaoto.2013.3044>, URL <http://archotol.jamanetwork.com/article.aspx?doi=10.1001/jamaoto.2013.3044>.
- [62] MacKenzie DS. Four basic types of fracture mechanisms | gear solutions magazine your resource to the gear industry. 2020, URL <https://gearsolutions.com/departments/hot-seat/four-basic-types-of-fracture-mechanisms/>.
- [63] Alshabib A, Jurado CA, Tsujimoto A. Short fiber-reinforced resin-based composites (SFRCs); current status and future perspectives. *Dent Mater J* 2022;41(5):647–54. <http://dx.doi.org/10.4012/dmj.2022-080>.
- [64] Sui N, Yan X, Huang TY, Xu J, Yuan FG, Jing Y. A lightweight yet sound-proof honeycomb acoustic metamaterial. *Appl Phys Lett* 2015;106(17). <http://dx.doi.org/10.1063/1.4919235>.
- [65] Wareing RR, Davy JL, Pearce JR. Variations in measured sound transmission loss due to sample size and construction parameters. *Appl Acoust* 2015;89:166–77. <http://dx.doi.org/10.1016/j.apacoust.2014.10.001>.
- [66] Tan WH, Sin CF. Sound transmission loss analysis on building materials. *Int J Automot Mech Eng* 2018;15(4):6001–11.
- [67] Warnock ACC. *Fundamentals of building acoustics*. National Research Council of Canada. Institute for Research in Construction; 1985.
- [68] Liu X, Dong C, Li S, Cong X, Wang X, Rudd C, Yi X, Liu X. Novel design of skin construction on the sound absorption of honeycomb sandwich panels. *Compos Struct* 2025;356(July 2024):118870. <http://dx.doi.org/10.1016/j.compstruct.2025.118870>.
- [69] Arjunan A, Baroutaji A, Robinson J, Vance A, Arafat A. Acoustic meta-materials for sound absorption and insulation in buildings. *Build Environ* 2024;251(January):111250. <http://dx.doi.org/10.1016/j.buildenv.2024.111250>.

- [70] Liu Z, Dong C, Tong L, Rudd C, Yi X, Liu X. Sound absorption performance of ultralight honeycomb sandwich panels filled with “network” fibers—*Juncus effusus*. *Polymers* 2024;16(13). <http://dx.doi.org/10.3390/polym16131953>.
- [71] Bahrami M, Abenojar J, Martínez MÁ. Recent progress in hybrid biocomposites: Mechanical properties, water absorption, and flame retardancy. 2020, <http://dx.doi.org/10.3390/ma13225145>.
- [72] Fatima S, Mohanty AR. Acoustical and fire-retardant properties of jute composite materials. *Appl Acoust* 2011;72(2–3):108–14. <http://dx.doi.org/10.1016/j.apacoust.2010.10.005>.